18TH WORLD CONFERENCE ON EARTHQUAKE ENGINEERING
WCEE2024
MILAN

MILAN, ITALY
30TH JUNE - 5TH JULY 2024

www.wcee2024.it

SIMULATION OF A SCENARIO DATABASE OF CONSISTENT GROUND MOTIONS FOR SITE SPECIFIC EARTHQUAKE RESPONSE

L. Alvarez Sanchez[1], I. Zentner[2]

[1] EDF R&D, Paris, France, luis-guillermo.alvarez-sanchez@edf.fr

[2] EDF R&D, Paris, France

Abstract: *Acceleration time histories are a key ingredient when conducting nonlinear structural response analysis for the purposes of as seismic risk assessment. Their importance lies in their function as a link between the hazard at the site and the structural response. Ideally, the selection of recorded accelerograms should account for causative seismological parameters in agreement with the scenarios corresponding to the distributions of target IMs obtained from Probabilistic Seismic Hazard Analysis (PSHA). Since time history response analysis of complex or nonlinear structures are generally time consuming, care needs to be taken in the selection of the smallest set of accelerograms that are hazard consistent and suitable for engineering. Nevertheless, this task is often not an easy one as databases of recorded ground motions are scarce for specific scenarios, especially for large magnitude, close distant scenarios, and for specific site conditions, such as for example rock sites. To overcome these limitations, synthetic ground motions have been considered as candidates to generate a scenario database for site specific risk assessment. Specifically, physics-based stochastic ground motion simulation methodologies represent an attractive alternative due to their ease of application and physical meaning of the input parameters considered by these models. To illustrate such an application, this study presents the construction of a database of simulated ground motions to be used for earthquake response analysis for a site in the region of central Italy. The database of simulated ground motions is populated by synthetics obtained by means of 3D stochastic simulation, considering both P and S-wave waves and a simplified 1D layer propagation scheme. To this end, distributions of meaningful input parameters were obtained from the literature and by the study of earthquake ground motions recorded in the region of interest. Next, the parametrized model is used to generate a database of ground motions and finally a set of comprehensive comparisons, carried out in terms of several intensity measures (IMs) of interest, is used to evaluate the representativeness of the simulated database. Special focus is given to the propagation of the uncertainty to capture the repeatability of the IMs of the simulated earthquake ground motions as modelled by valid ground motion models.*

1 Introduction

The availability of earthquake ground motion, consistent with the hazard expected at a site, is of vital importance in the context of earthquake risk assessment. These ground motions are usually considered in the form of acceleration time histories and their importance lies in their use as link between the hazard and the structural response. Databases of these earthquake ground motions, however, are often scarce and are incomplete for a wide range of scenarios of interest. One of such cases, for which earthquake ground motion data is scarce, is that of rock-like sites. In fact, most strong-motion databases contain earthquake recordings of stations installed on soil or soft-rock sites, while very few stations are on hard-rock sites. Here a different issue rises, the definition of the features of the “rock” site also depends in the intended application, (Lanzano, Felicetta, Pacor, Spallarossa, & Traversa, 2022), this however is a

different subject and is out of the scope of this study. One of the most typical applications, however, is that of the definition of a reference rock (Steidl, Tumarkin, & Archuleta, 1996), i.e., with a flat/unamplified response over a frequency range of engineering interest, where site-effects are to be added subsequently according to soil response analysis.

To circumvent the shortage of recorded ground motions at reference rock sites, researchers and practitioners have considered recordings from both rock and soil sites, and from databases of simulated ground motions. Studies such as Garcia de Quevedo Inarritu et al., (2023), and Alvarez et al., (2023) have looked at the implications of such considerations in terms of risk analysis of single structures. The results obtained from these studies indicate that, when carefully selected considering the conditional spectra method (Baker, 2018), the response obtained from running the selected sets of records through the studied structures did not vary significantly between sets of rock and soils sites, and sets of recorded and simulated ground motions, respectively. Nonetheless, the consideration of recordings from soil sites often requires considerable scaling factors to achieve the spectral amplitudes related to the target rock site spectra, thus requiring an important (and not physical) modification of the recorded ground motions (Huang, Whittaker, & Hamburguer, 2011), (Garcia de Quevedo, Sipcic, Alvarez Sanchez, Kohrangi, & Bazzurro, 2023). One of the most viable alternatives to avoid such scaling of ground motions, and to remain closest to the range of scenarios dictated of simulated ground motions generated specifically for the target context.

To explore the potential of simulated ground motions, the METIS project (metis-h2020.eu), whose may objective is the development and improvement of tools and methodologies employed in seismic safety assessments of nuclear reactors, focused its attention in the generation of databases of synthetic ground motion time histories on bedrock.. As a first step, Deliverable D4.3 (Akazawa, et al., 2023) summarizes a series of ground motion simulation methodologies considered within the project. One of such method is the 3D stochastic ground motion simulation methodology originally presented by Otarola et al., (2016) and Ruiz et al., (2018), and later modified by Alvarez (2022). This ground motion simulation technique builds over other stochastic methods such as those presented in Boore (1983), Boore (1996)and Motazedian et al., (2005), by incorporating a model for the full body wave field spectra (i.e., P, SV and SH-waves). Another advantage of this technique is the physical meaning of the parameters used in the construction of the synthetic ground motions, this feature allows a direct link between seismicity recorded at the region and subsequent simulations, using source and path terms consistent with the ones used to compute seismic hazard. Finally, applications such as that presented in Alvarez et al., (2023) have demonstrated the compatibility of the technique for the generation of databases of simulated ground motions to be used for earthquake response assessment.

This study presents the implementation of the 3D stochastic ground motion simulation methodology for the generation of a database of simulated ground motions to be used in the earthquake risk assessment of the METIS case study. The first section of this document introduces the ground motion simulation technique. Next, the METIS case study is introduced alongside a set of ground motions recorded in the region of interest, considered as reference in the derivation of the input parameters required for the simulation of ground motions with the herein considered technique. Afterward, the calibration of the simulation technique is shown and assessed by comparing simulated and reference recorded ground motions in the region of the case study. Finally, the calibrated model is used to generate a database of simulated ground motions, populated with new earthquake scenarios consistent with those obtained from the disaggregation of the hazard computed for the METIS case study. The database of simulated ground motions is then contrasted with ground motion models relevant for the area of interest. Perspectives on different applications and improvements are provided in the end of this document.

2 3D Stochastic Ground Motion Simulation Technique

The ground motion simulation method presented in this section, and from here on referred to as SGMSM, is a modified version of the stochastic technique introduced in Otarola & Ruiz, (2016) and Ruiz et al., (2018), and modified to include a more realistic representation of the source and the inter-frequency correlation structure of the spectral amplitudes.

The stochastic ground motion simulation method proposed in Otarola & Ruiz, (2016) and Ruiz et al., (2018) computes time histories in the frequency domain and model the Fourier Amplitude Spectrum (FAS) as a convolution of modulated noise with a random phase and a mean ground motion spectrum:

$$FAS = U(f, r, M_0)\sqrt{S_0} \tag{1}$$

Where U is the mean simulated ground motion spectrum, S_0 is the white noise with normalized power spectral density, f is the frequency, r is the source-receiver distance, and M_0 is the source seismic moment. Considering a finite-source model, where the source is discretized into an array of point-sources, time histories are constructed as the lagged summation of the individual sub faults contributions, (Atkinson et al., 2009; Beresnev & Atkinson, 1997; Motazedian & Atkinson, 2005). The definition of the mean simulated ground motion spectrum, for wave type w (P, SV, and SH), sub-source i and component d (vertical, radial, and tangential) is shown in the following equation:

$$U_i^w{}_d\left(f, r_i, M_{0_i}\right) = C^w{}_{i_d}(, M_{0_i})\, S^w{}_i(f) A^w{}_i(r_i, f) Z^w{}_{i_d}(f) \tag{2}$$

Where $\mathrm{C}^{\mathrm{w}}{}_{i_d}$ is the scaling constant, $S^w{}_i(f)$ represents the source, $A^w{}_i(r_i, f)$ the propagation (attenuation due to the path) and $\mathrm{Z}^{\mathrm{w}}{}_{i_d}(f)$ the site-specific effects component of the simulated ground motion spectrum. The full description of the formulation of each of these components can be found in Alvarez (2022).

The phase of the simulated ground motions is included by mean of the band limited Gaussian white noise with finite duration. A modulating function is applied to the white noise with the intention to include the characteristic temporal non-stationary nature of ground motion time series. The Saragoni and Hart (1973) modulating function, $\omega(t, e, \eta, t_\eta)$, shown in equation (3) is often considered in stochastic simulation methods, e.g., Otarola et al., (2016) and Ruiz et al., (2018), and was also considered in this study.

$$\omega(t, \zeta, \eta, t_\eta) = a\left({}^{t}/_{t_\eta}\right)^b \exp\left(-c\left({}^{t}/_{t_\eta}\right)\right) \tag{3}$$

Where ζ and η are parameters defining the shape of the function, $a = e^{1/\zeta}$, $b = \zeta \ln(\eta)/(1 + \zeta(\ln(\zeta) - 1))$, $c = b/\zeta$, $t_\eta = f_{Tgm} \cdot T_{gm}$. T_{gm} is the duration of the signal for the computation of the window function, and f_{Tgm} is a factor modelling the elongation of the windows. Previous implementations of this modulating function have considered different combinations of parameters. These, however, are often adjusted for matching reference signals, e.g., Otarola et al., (2016) and Ruiz et al., (2018) More details on this procedure may be found in Alvarez (2022) and Akazawa et al., (2023).

3 METIS case study

The case study of the METIS project was defined to demonstrate the methods and tools tested within the context of the project. This case study considers a hypothetical nuclear facility located in the western coast of Tuscany (coordinates 11.202E, 42.424N). The hazard at the site of the case study was estimated by means of PSHA (Cornell, 1968), following the methodology described in Chartier et al., (2023) and for a site with *Vs30 = 1000 m/s*. The hazard curves for the site may be consulted in METIS report MSH7 (Chartier & Rood, 2023).

The role of simulated ground motions within the case study is of providing supplementary input acceleration time histories for structural response analysis. Because acceleration time histories may theoretically be simulated at any desired location, the advantage of a database of simulated ground motions lies in the capacity to provide the specific scenarios missing in the database of recorded ground motions.

3.1 Reference recorded ground motions

Regardless of the considered simulation technique, ground motions contained within the simulated database should be consistent with ground motions recorded at the region around the site of the case study. To achieve this objective, a set of ground motions recorded at the region of interest, and selected from the ESM database, (Lanzano G, 2019), were first studied to derivate distributions of meaningful

input parameters to be considered in tandem with an application specific calibration of the ground motion simulation technique.

The set of reference recorded ground motions was selected considering a region of interest delimited by parallels 41N and 43.5N, and by meridians 11E and 15E. Figure 1 shows the location of: i) the site of the case study, ii) the epicentres, and iii) recording stations for the herein considered set. The reference ground motions were categorized by their magnitude and recording site characteristics. In agreement with the hypothesis of the PSHA conducted for the site this study considers only events with magnitudes above 4.0 ($M_w \geq 4.0$) and sites with an average shear wave velocity of the upper 30m (*Vs30*) above 1000 m/s ($Vs30 \geq 1000$ *m/s*). Figure 1 shows the relative location of the epicentres of the earthquake events and stations considered in this study, alongside the distributions of causative and site parameters of the recorded events considered in this study.

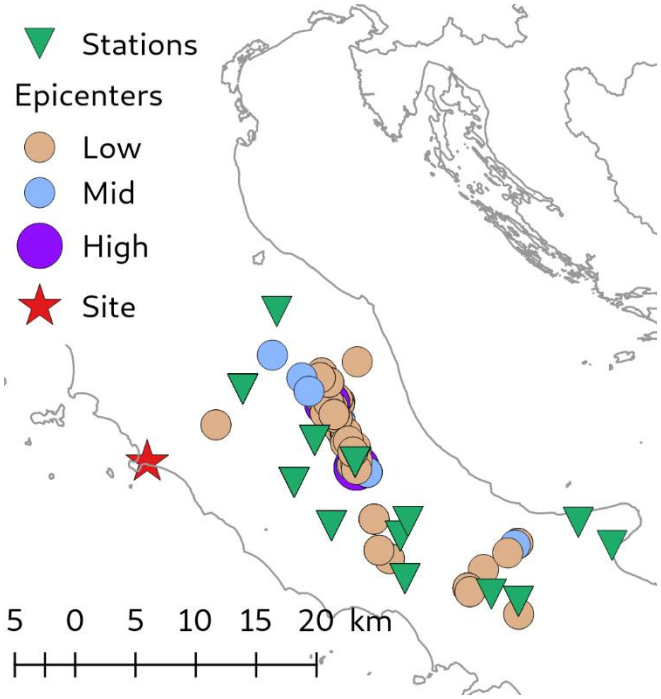

Figure 1. Locations of the epicenters (circles) and stations (triangles) in the area of interest. The location of the site of the case study is marked with a red star. In the figure, the magnitude of the earthquakes is shown by the color of the marker, where low magnitude is considered for 4.0 < $M_w \leq$ 5.0, mid magnitude for 5.0 < $M_w \leq$ 6.0, and high magnitude for 6.0 < M_w

All downloaded time histories were treated before any manipulation. The processing of the time histories consisted of the following steps: i) Base line correction by subtraction of the average of the time series, ii) 5% cosine tapering at the beginning and at the end of the signal, and iii) Application of a bandwidth (acausal) filter to eliminate the low-frequency noise and the response of the measuring instrument.

4 Input parameters for ground motion simulation

The generation of synthetic ground motions with the SGMSM requires the definition of a series of parameters/models. These are: i) the parameters defining the simulated ground motion spectrum, ii) the parameters defining the duration and time modulating functions characterizing the time histories, iii) the source (geometry and slip) and finally iv) crustal models. The following sections describe each of these individual inputs as defined from the study of a set of reference recorded ground motions or references found in the literature.

4.1 Ground Motion duration

The duration of the simulations for each point source composing the source model, T_{gm}, was considered as the significant duration of the ground motion (Ds_{5-95}). For the purposes of this study, this parameter

was defined as the duration between the instants where 5% and 95% of the Arias Intensity, *AI*, is reached.

The model describing these durations was defined based on the study of ground motions recorded in the region. Figure 2a shows the distribution of Ds_{5-95} *vs* R_{hyp} for the considered set. Also included in the figure is the median of the regressions conducted for three subsets selected based on different magnitude bins, i.e., $4 < M_w \leq 5,\ 5 < M_w \leq 6,\ 6 < M_w$. Due to the similarity of the regressions for the lowest magnitude bins, only two models are kept: i) one for events with magnitude below 6.0 ($6 \geq M_w$) and shown in equation (4), and ii) a model for events with magnitudes above 6 ($6 < M_w$) and shown in equation (5).

$$log_{10}(T_{gm}) = 0.67 log_{10}(R_{hyp}) - 0.27 + N(0, 0.15) \quad (4)$$

$$log_{10}(T_{gm}) = 0.357 log_{10}(R_{hyp}) + 0.582 + U(-0.1, 0.1) \quad (5)$$

The definition of the modulating functions shaping the acceleration time history in the time domain is discussed in coming sections detailing the calibration of the SGMSM.

4.2 Ground Motion Spectrum

As reference, this study considered the seismological characterization of central Italy reported in Morasca et al., (2023). Here, the authors present distributions of the input parameters describing the source, attenuation and site components of earthquake ground motions as obtained from the inversion of earthquake spectra. The referenced study considered more than 30000 waveforms recorded from 456 earthquakes by about 460 stations located in the proximity of the site of the METIS case study.

According to the authors, the studied earthquake events were characterized by two different distributions of stress drop. The first distribution was defined for events with a moment magnitude (M_0) below 6.4e16 N-m, and the second one for events with a moment magnitude above 10e17 N-m. Equations (6) and (7) show regressions performed as part of this study with the data reported by the authors for each of these distributions, respectively (see Figure 2b for a comparison for the lowest magnitude range). The source spectra reported by the authors is completed with the consideration of the high-frequency attenuation function parametrized by κ_{SRG} and introduced first in Anderson et al., (1984) (typically considered as part of the attenuation model, i.e., Boore (2003)). The model regressed from the values of κ_{SRG}reported by the authors is shown in (8). A comparison of the mean of the regressed models and the values obtained in Morasca et. al., (2023), for the lowest magnitude range, may be seen in Figure 2c

$$log_{10}(\Delta\sigma) = 0.380(\pm 0.063) log_{10}(M_0) - 5.748(\pm 0.972) \quad (6)$$

$$log_{10}(\Delta\sigma) = 0.088(\pm 0101) log_{10}(M_0) - 0.545(\pm 1.814) \quad (7)$$

$$log_{10}(\kappa_{SRG}) = 0.1710 log_{10}(M_0) - 4.279 + N(0{,}0.1710) \quad (8)$$

Regarding the attenuation, Morasca et. al., (2023) reported a bilinear geometrical attenuation function with a hinge at 70 km (see equation (9)). Regarding the quality factor, the authors considered a function of the form $Q^S(f) = Q_0 f^M$, where $Q_0 = 247 \pm 12.8$ and $M = 0.38 \pm 0.03$.

$$G(R_{hyp}) = \begin{cases} \left(\frac{10}{R_{hyp}}\right)^{1.77} & R_{hyp} \leq 70\ km \\ \left(\frac{10}{70}\right)^{1.77} \left(\frac{70}{R_{hyp}}\right)^{0.56} & R_{hyp} > 70\ km \end{cases} \quad (9)$$

Finally, no site-effects were considered in the representation of the FAS because the objective of this application is to generate reference acceleration ground motion for site specific analysis. It is important to highlight that, according to the theory behind the Generalized Inversion technique, e.g., (Oth, Parolai, & Bindi, 2011), this calibration results in simulated ground motion spectra consistent with the station (or combination of stations) used to define the reference condition to separate source and site contributions. The combination of stations considered by the authors results in a mean Vs_{30} = 900 m/s.

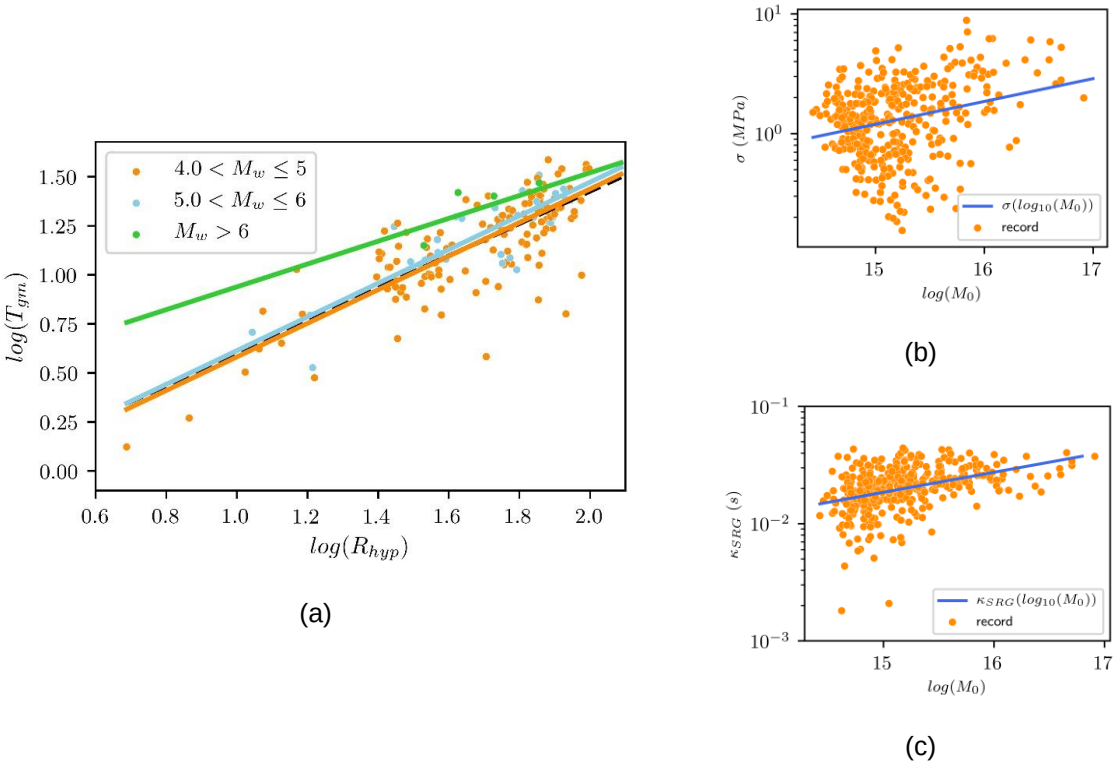

Figure 2. (a) - Distribution of the significant duration of ground motions recorded at the region of the case study. Distribution of the (b) - stress drops, Δσ, and (c)- high-frequency attenuation parameter, κ_{SRG}, reported in Morasca et al., (2023) for events with a moment magnitude below 6.4e16 N-m. The figures also include the median of the models regressed as part of this study.

1.1. Crustal structure

The model of the crust contemplated in this study is that of Li et al., (2017). Here, the authors report a series of layered velocity models for the crust in different regions of Italy. The models are based on the inversion of locally recorded data and include the uncertainty related to the depth and wave-propagation velocities at each of the layers of the model. Figure 3 shows the herein considered crust model.

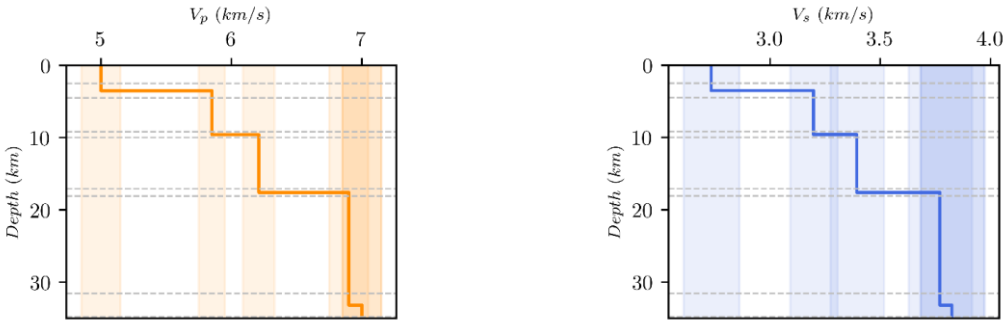

Figure 3. Regional layered model for the crust (Li et al., 2017). Wave propagation velocities of (a) – P waves, and (b) – S waves. In the figure the dashed lines represent the range of variability of the depth of the interphases and the shadowed region that of the propagation velocities

1.2. Source model

Each of the events simulated in this study was generated with a finite source model. The variability of their geometry was considered with the relationship proposed by Wells & Coopersmith (1994), where the length and width of the fault depend on the size and mechanism of the rupture. To complement the geometry of the source, each of the fault planes was oriented with dip and strike angles sampled randomly from uniform distributions varying between 10°-90° and 0°-359°, respectively. Regarding the

definition of the slip distribution, this study considered the kinematic source model reported Ruiz et al., (2011) to generate distributions of 1000 asperities uniformly distributed along the rupture surface. Finally, the propagation of the rupture in each of the conceived sources was modelled with the algorithm reported in Gallovič et al., (2016).

1.3. Calibration of the SGMSM

The characterization of the SGMSM was completed by calibration of the technique to adjust the shape of simulated acceleration time histories and the amplitude of the ground motion movement. In the preliminary phase of this work, the lack of a site-specific parametrization for the time modulating functions, and the use of the stress drop distributions reported in Morasca (2023) resulted in simulated ground motions with unrealistic durations and overly large high-frequency content. To remedy these deviations this study implemented the calibration procedure proposed in Alvarez (2022). Here differences between the IMs of interest extracted from the set of reference recorded ground motions and those extracted from sets of synthetic ground motion replicas computed with different combinations of the target modelling parameters are minimized.

Same as in Alvarez (2022), this study considered the proposed iterative calibration procedure to optimize the following modelling parameters: (i) the time modulating window parameters, i.e., ζ, η and f_{Tgm}, modelling the location of the peak, attenuation, and elongation of the window; and (ii) the stress drop defining the source. The replicas used in the calibration were constructed by generating one simulated ground motion per record in the reference recorded set using the same causative parameters, i.e., M_w, R_{hyp}, and Z_{hyp}, of the recorded ground motion. The difference in the recorded and simulated ground motions in terms of the j^{th} Intensity Measure (IM) can be defined by equation (10).

$$\varepsilon_{ij} = ln\left(IM_{ref,_{ij}}\right) - ln\left(IM_{sim,_{ij}}\right) \tag{10}$$

Here, $IM_{ref,ij}$ and $IM_{sim,ij}$ show the corresponding values of the IMj in i^{th} pair of recorded and simulated ground motions. To find the total error of a set of simulated ground motions, one can compute the sum of the square of the error terms obtained by equation (10) for multiple IMs (i.e., total of N_{IM}) and for all the records in the database, N_{rec}, according to equation (11).

$$Error = \sum_{i=1}^{N_{rec}} \sum_{j=1}^{N_{IM}} w_j \cdot {\varepsilon_{ij}}^2 \tag{11}$$

Here, w_j represents a weighting factor allowing the prioritization of the match of IM_j, $j=1,\ldots, N_{IM}$ considered in this procedure. In this study, two calibration rounds were run to target each of the specific issues at hand. First, an initial calibration round targeting the amplitude of the ground motion was conducted, here only the Peak Ground Acceleration (PGA) of the Geometrical Mean (GM) of the Horizontal components was chosen as target IM (thus setting the weighting factor to 1.0). Next, a second round of calibration was run targeting the overall shape and duration of the simulated acceleration time histories, here a vector of 3 IMs was considered: $Ds_{5\text{-}95}$, $Ds_{5\text{-}75}$, and $Ds_{20\text{-}80}$ with weighting factors of 0.5, 0.25 and 0.25, respectively.

In this study, three different groups of ground motions were defined in recognition of the overall differences between the target IMs as a function of magnitude: low magnitude events ($4.0 < M_w \leq 5.0$), medium magnitude events ($5.0 < M_w \leq 6.0$), and high magnitude events ($6.0 \leq M_w$). The optimal set of parameters, for each group and calibration run, was searched a total of 10 times, each of which contemplated a different pool of likely combinations and overall random seeds in the generation of simulated ground motion and sampling of input parameters. This extra step was done to compensate for the finite number of combinations of target parameters and to sample the variability introduced by the uncertainty in the other input variables such as the attenuation and crustal medium. The simulation of the replicas followed an event-based approach, which means that all the simulated replicas coming from an earthquake scenario share the same source parameters, i.e., finite rupture model and source spectrum. Regarding the duration of the ground motion, each of the sub faults composing the finite source model is assigned a duration based on its estimated moment magnitude (proportional to the slip of the sub fault and the total slip of the fault), and the models detailed in section 4.1.

Figure 4 shows the distributions of stress drops obtained from the calibration procedure for the three defined groups. The figure includes the histograms and regressions conducted for the deduced populations of the parameter. The obtained results indicate that the three populations follow a log normal distribution with similar mean and standard deviation values. These results differ with respect to those reported in Morasca et al., (2023), where significantly different distributions were proposed for events with a seismic moment below 6.4e16 N-m *(M_0 < 6.4e16 N-m)*, and for events with seismic moment above 10e17 N-m *($Log_{10}M_0$ > 10e17 N-m).* These discrepancies were attributed to the differences between the SGMSM and the Brune model (Brune, 1970) considered in the regression conducted in Morasca et al., (2023). The discrepancies are mostly important for the highest magnitude group which lead to believe that differences are also due to the consideration of a finite fault source model within the generation of the simulated ground motions. In fact, the mean value for events within the low and mid magnitude groups fairly matches that reported by the authors. The results obtained for the calibration of the window parameters are not shown in this document due to the limited space available. These, however, may be found in Alvarez & Zentner (2023).

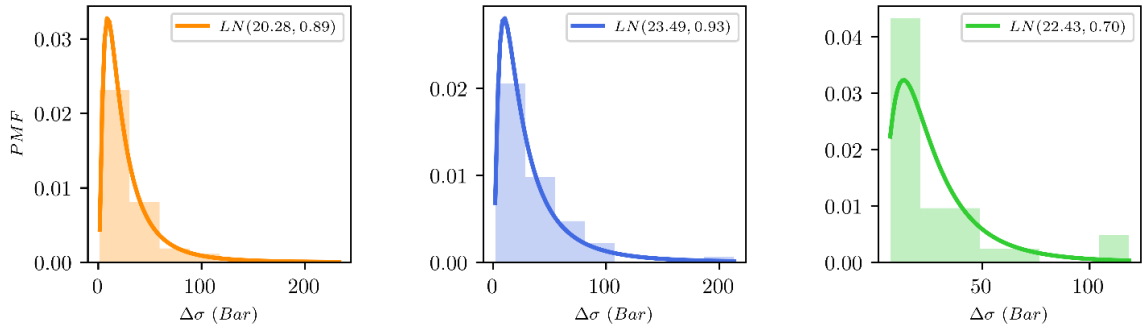

(a) (b) (c)

Figure 4. Distributions of stress drops obtained from the calibration procedure for (a) – Low, (b) – Mid, (c) – High magnitude earthquakes as defined in this report.

Figure 5 and Figure 6 show a comparison of several IMs considered (directly or indirectly) in the calibration procedure. Figure 5 shows indicates that there is good agreement between the response spectra of the geometrical mean of the horizontal components, Sa_{GM}, of recorded and synthetic replicas for the low and mid magnitude earthquakes, both in terms of mean and dispersion (here shown by the shaded area representing the space between the 16th and 84th percentiles of the distribution), and for periods of vibration up to 10s. The results obtained for the highest magnitude range, shown in Figure 5c, differ for the longest period range due to a more accentuated attenuation of the simulated ground motions. The short period content, however, shows a much more similar distribution when compared to the recorded references. Overall, these results are considered satisfactory because of the matching of the spectral content of reference and simulated ground motions at short period range, directly targeted during calibration procedure by searching for the distributions of stress drop resulting in matching peak ground accelerations.

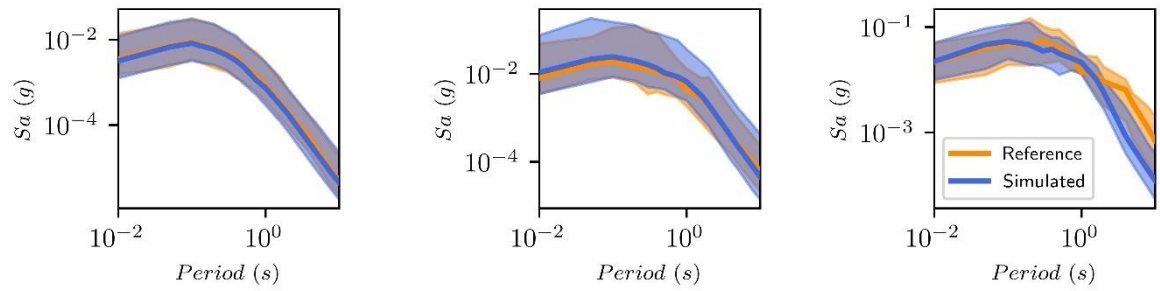

(a) (b) (c)

Figure 5. Comparison of response spectra of the geometrical mean of the horizontal components, Sa_{GM}, computed from the reference ground motions and the synthetic replicas generated at the end of the calibration procedure. (a) – Low, (b) – Mid, (c) – High magnitude earthquakes as defined in this report.

The comparison of the significant durations between reference ground motions and replicas, shown in Figure 6, indicates that the calibration procedure results in synthetic replicas with significant durations close to the reference ones. In general, the significant duration of the replicas oscillates around the reference values, however, in some cases, specifically for the highest magnitude group, the replicas result in durations smaller or larger than the reference values. These divergences may be attributed to effects related to the specific path taken by the seismic waves to arrive from source to site, specific source mechanisms not captured by a simplistic clustering based only on magnitude or even the fact that the considered modulating function model may not be fully adequate for simulations such as the ones conducted in the application discussed herein.

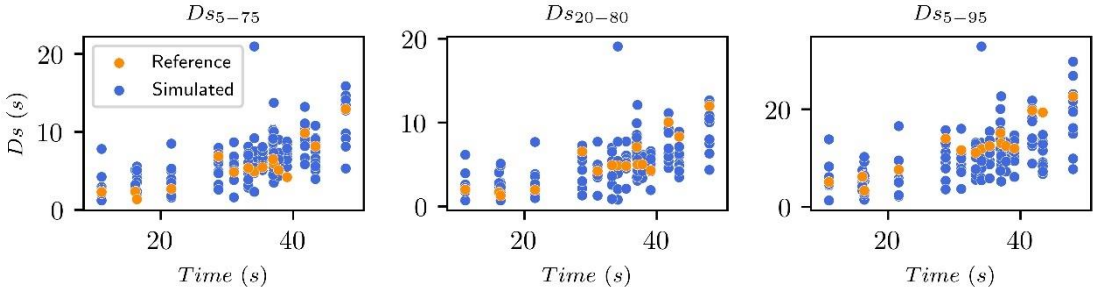

Figure 6: Comparison of three different durations ($Ds_{5\text{-}95}$, $Ds_{5\text{-}75}$, and $Ds_{20\text{-}80}$) for the mid magnitude earthquakes. Homologue figures are included in the supplementary material for the other groups.

5 Database of simulated ground motions

The calibrated SGMSM can be employed to generate simulated ground motions consistent with the ones recorded in region of interest (at least in terms of the IMs considered in the calibration procedure). To illustrate the use of the calibrated SGMSM, a simulated database, herein referred to as SDB, was generated. The SDB was populated with over 8000 3D acceleration time histories generated by conceiving earthquake scenarios sampled from a uniform magnitude distribution (4 ≤ Mw ≤ 6) and for a maximum hypocentral distance of 60 km. These causative parameters were selected to be consistent with the disaggregation of the hazard at the site of the case study detailed in the report “MS7: PSHA output for METIS case study” (Chartier et al., 2023).

The time histories populating the SDB were generated with the same event-based approach described in section 1.3. Once again, no site-effects were considered because the objective of this application is to generate reference acceleration ground motion for site specific analysis. Figure 7 shows the attenuation of three different spectral amplitudes (Sa = PGA, 0.2s, and 1.0s) for all simulated ground motions in the SDB.

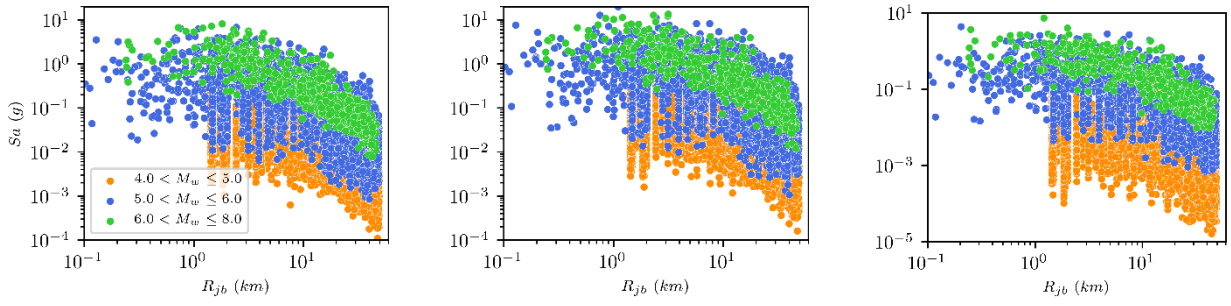

(a) (b) (c)

Figure 7: Attenuation of the spectral accelerations of the events populating the SDB at different periods of vibration: (a) PGA, (b) 0.2s, and (c) 1.0s.

A comparison of the attenuation of the spectral, for three different magnitude bins, and three periods of vibration, is shown in Figure 8. The figures shown the spectral acceleration from: i) the SDB (marked as simulated), ii) the recorded reference ground motions (marked a recorded), and iii) the predictions given by the GMMs considered in the PSHA computations for the case study (Chartier & Rood, 2023): These are: the ESHM20 (Kotha et al., 2020) and the modified model reported in Lanzano et al., (2019) and

modified to include the reference rock correction factor reported in Lanzano et al., (2022). The results shown in the figure indicate that the distributions of spectral accelerations computed from the simulated ground motions matches that of the recorded ones for most cases, for these two sets, the largest differences were found in the longer period (1.0s) and for the higher magnitude bin. These differences were expected because of the differences noticed in the calibration procedure (see Figure 5), and are mostly attributed to the simplicity of the rupture and wave propagation considered in stochastic ground motion simulation models, (Akazawa, et al., 2023), and the lack of recorded scenarios to exploit as training data for target scenarios with these causative parameters. This magnitude bin and period of vibration also result in the largest discrepancies between simulated ground motions and predictions from the reference GMMs. In fact, apart from this latter case (high magnitude and long period of vibration) and that of lowest magnitude bin and longest period of vibration (where simulated ground motions are closer to data), the comparison with respect to the GMMs was found to be rather good.

Finally, Figure 9 shows the comparisons of the comparison of the significant durations considered in the calibration process for the reference and simulated ground motions, and the estimations from the GMM proposed in Afshari et al., (2016). The comparisons show that the simulated ground motions follow the functional dictated by the GMM, and where recordings area available, also the trend shown by these records.

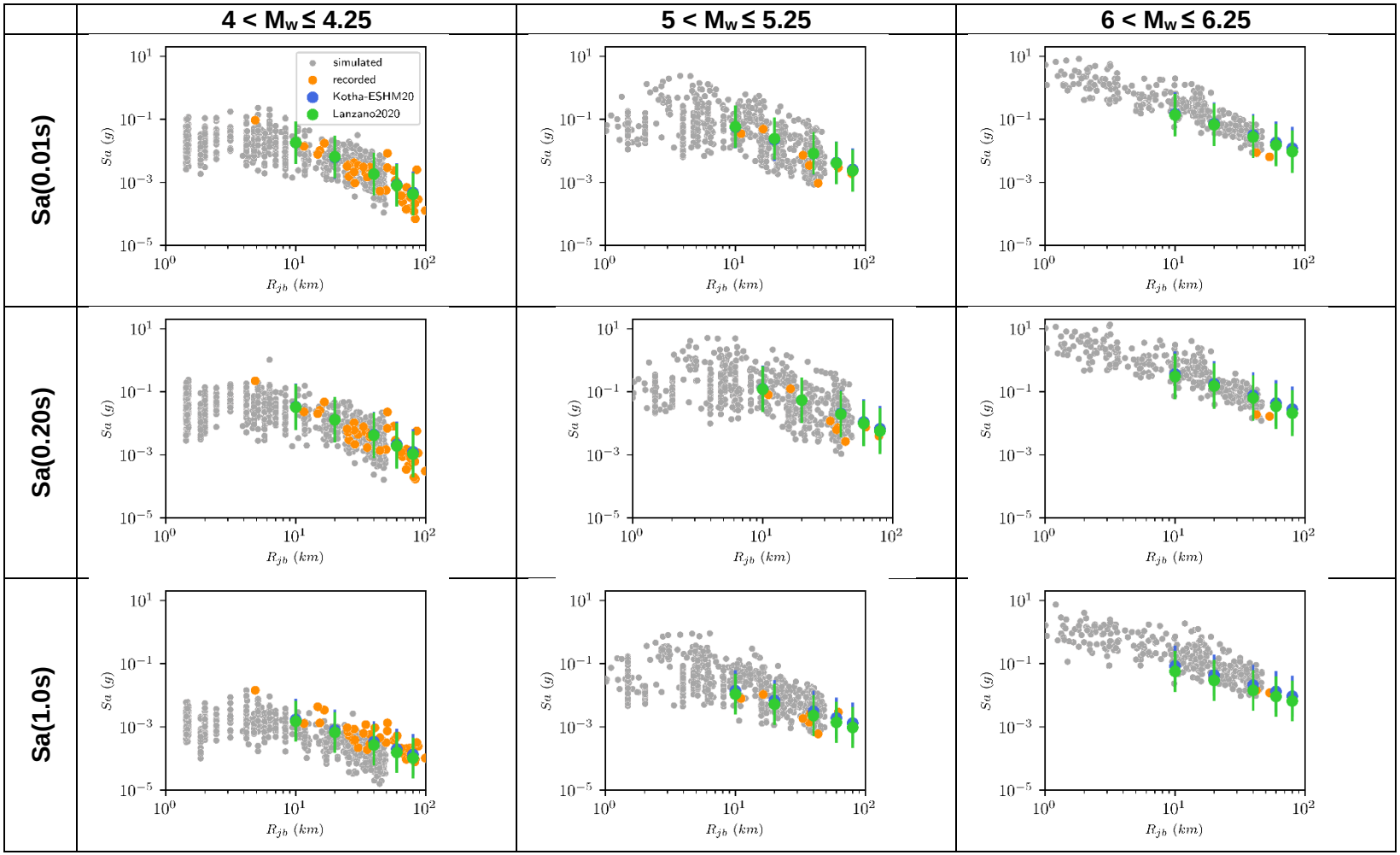

Figure 8: Comparison of the attenuation of the spectral accelerations for the RotD50 component (at different periods of vibration) of the events populating the SDB, and the recoded reference events. The figure inlculdes also the estimations given by the ESHM20 (Kotha, Weatherill, Bindi, & Cotton, 2020) *and the modified Lanzano et al.* (2022) *ground motion models, here the marker signals the medium and the bars the intervals between the 5th-95th percentiles.*

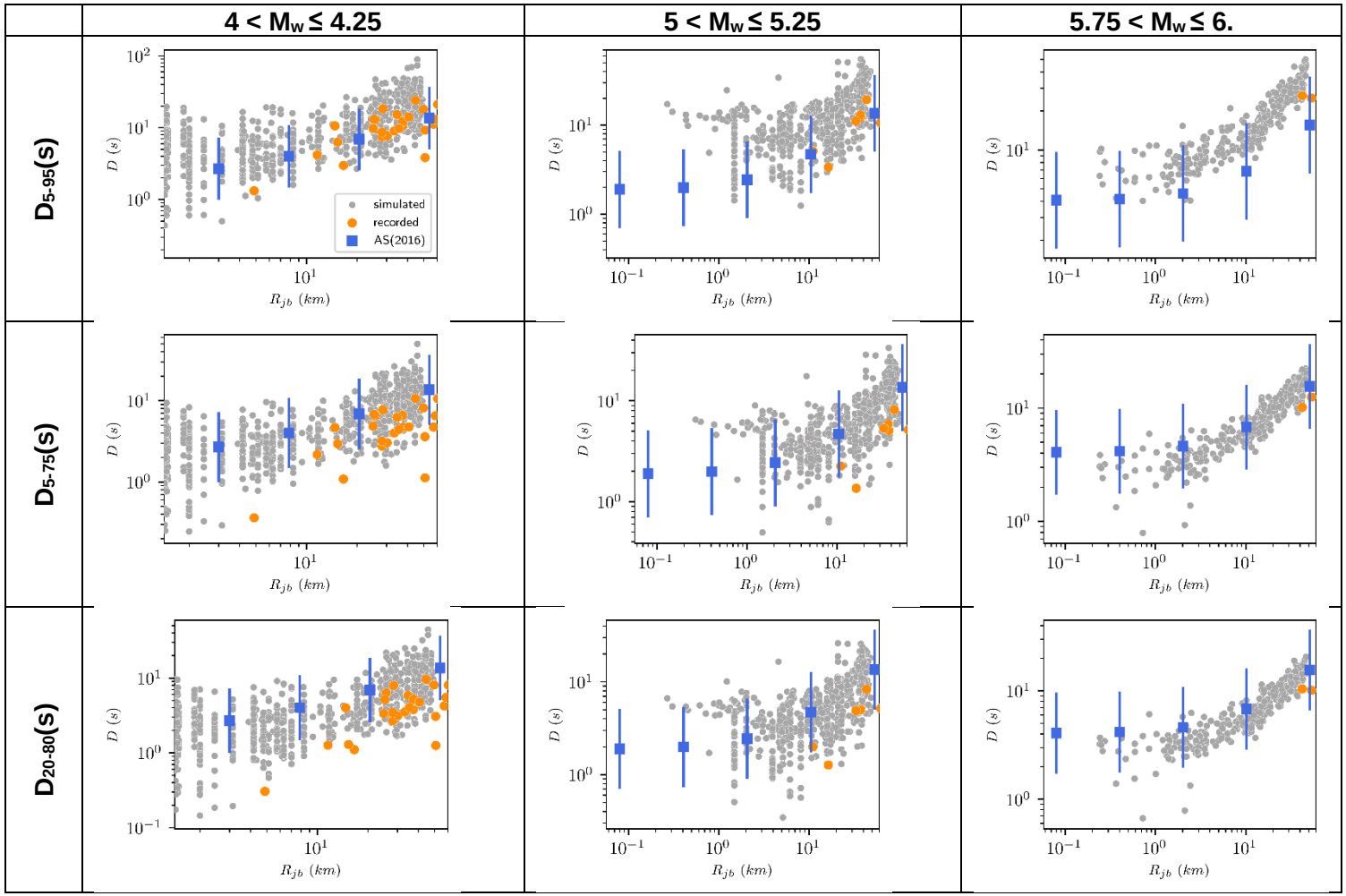

Figure 9: Significant durations for the GM component of ground motions populating the SDB, the AS(2016) ground motion model, and ground motions recorded at the region of interest.

6 References

Afshari, K., & Stewart, J. (2016). Physically Parametrized Prediction Equations for Significant Duration in Active Crustal Regions. *Earthquake Spectra*, 32, 2057–2081. https://doi.org/10.1193/063015EQS106M.

Akazawa, T., Alvarez Sanchez, L., Ameri, G., Baumont, D., Cotton, F., Irikura, K., . . . Zentner, I. (2023). *Methodologies for physics-based simulation of ground motion: Analysis of different approaches and applications to METIS case study.* METIS.

Alvarez Sanchez, L. (2022). *Improved 3D Ground Motion Simulation for Structural Response Analysis.* Paris: Université Gustave Eiffel - Thesis.

Alvarez Sanchez, L., & Zentner, I. (2023 (work on progress)). *Methodologies for physics-based simulation of ground motion: Simulated database for the METIS case study.* Paris: METIS.

Alvarez Sanchez, L., Quevedo de Inaritu, P., Sipcic, N., Kohrangi, M., & Bazzurro, P. (2023). Hazard-consistent simulated earthquake ground motions for PBEE applications on stiff soil and rock sites. *Earthquake Engineering & Structural Dynalics*, doi.org/10.1002/eqe.3987.

Anderson, J., & Hough, S. (1984). A MODEL FOR THE SHAPE OF THE FOURIER AMPLITUDE SPECTRUM OF ACCELERATION AT HIGH FREQUENCIES. *Bulletin of the Seismological Society of America*, 74 (5): 1969–1993. doi: https://doi.org/10.1785/BSSA0740051969.

Baker, J. W. (2018). An Improved Algorithm for Selecting Ground Motions to Match a Conditional Spectrum. *Journal of Earthquake Engineering*, 22(4), 708–723.

Boore, D. (1983). Stochastic Simulation of High-Frequency Ground Motions based on Seismological Models of the Radiated Spectra. *Bulletin of the Seismological Society of America*, 73(6).

Boore, D. (1996). SMSIM – Fortran Programs for Simulating Ground Motions from Earthquakes. *US Geological Survey*, Open-File Rept. 96-80-A, 96-80-B, 73 p p .

Boore, D. (2003). Simulations of ground motion using the stochastic method. *Pure and Applied Geophysics*, 160:635-676.

Boore, D. (2005). On pads qnd filters: Processing strong motion data. *Bulletin of the Seismological Society of America*, 95(2); 745-750. https://doi.org/10.1785/0120040160.

Brune, J. (1970). Tectonic Stress and the Spectra of Seismic Shear Waves from Earthquakes. *Journal of Geophysical Research*, 75: 4997-5009 - doi:10.1029/JB075i026p04997 .

Chartier, T., & Rood, A. (2023). *MS7: PSHA output for METIS case study.* METIS.

Cornell, A. (1968). Engineering seismic risk analysis . *Bulletin of the Seismological Society of America*, 1583-1606.

Douglas, J., & Aochi, H. (2008). A survey of techniques for prediction earthquake ground motions for engineering purposes. *Surveys in Geophysics*, 29(3):187-220 - https://doi.org/10.1007/s10712-008-9046-y.

Gallovič, F. (2016). Modeling velocity recordings of the mw 6.0 south napa, California, earthquake: Unilateral event with weak high-frequency directivity. *Seismological Research Letters*, 87(1): 2–14. DOI: 10.1785/0220150042.

Garcia de Quevedo, P., Sipcic, N., Alvarez Sanchez, L., Kohrangi, M., & Bazzurro, P. (2023). A closer look at hazard-consistent ground motion record selection for building-specific risk assessment: Effect of soil characteristics and accelerograms' scaling. *Earthquake Spectra*, 1303-1327 doi.org/10.1177/87552930231187407.

Huang, Y., Whittaker, A., & Hamburguer, R. (2011). Scaling earthquake ground motions for performance-based assessment of buildings. *Journal of Structural Engineering*, (3):311-321 - https://doi.org/10.1061/(ASCE)ST.1943-541X.0000155.

Kotha, S., Weatherill, G., Bindi, D., & Cotton, F. (2020). A regionally adaptable ground motion model for shaloow crustal earthquakes in Europ. *Bulletin of Earthquake Engineering*, 18: 4091-4125 - https://doi.org/10.1007/s10518-020-00869-1.

Lanzano G, S. S. (2019). The pan-European Engineering Strong Motion (ESM) flatfile: compilation criteria and data statistics. *Bulletin of Earthquake Engineering*, 17(2): 561-582 DOI: 10.1007/s10518-018-0480-.

Lanzano, G., Felicetta, C., Pacor, F., Spallarossa, D., & Traversa, P. (2022). Generic-To-Reference Rock Scaling Factors for Seismic Ground Motion in Italy. *Bulletin of the Seismological Society of America*, 112(3): 1583-1606.

Li, H., Michelini, A., Zhu, L., Bernardi, F., & Spada, M. (2017). Crustal velocity structure in Italy from analysis of regional seismic waveforms. *Bulletin of the Seismological Society of America*, (97). 2024-2039. DOI:10.1785/0120070071.

Morasca, P., D'Amico, M., Sgobba, S., Lanzano, G., Colavitti, L., Pacor, F., & Spallarossa, D. (2023). Empirical corrzlations between an FAS non-ergodic ground motion model and a GIT derived model for Central Italy. *Geophysical Journal International*, 233, 51-68.

Motazedian, D., & Atkinson, G. (2005). Stochastic finite-fault modeling based on a dynamic corner frequency. *Bulletin of the Seismological Society of America*, 95(3): 995-1010.

Otarola, C., & Ruiz, S. (2016). Stochastic generation of accelerograms for subduction earthquakes. *Bulletin of the Seismological Society of America*, 106(6): 2511-2520 - https://doi.org/10.1785/0120150262.

Oth, A., Parolai, S., & Bindi, D. (2011). Spectral analysis of K-NET and KiK-net data in Japan, Part I: Database compilation and peculiarities. *Bulletin of the Seismological Society of America*, 101(2), 652–666. https://doi.org/10.1785/0120100134.

Ruiz, S., Ojeda, J., Pastén, C. O., & Silva, R. (2018). Stochastic strong-motion simulation in borehole and on surface for the 2011 m w 9.0 tohoku-oki megathrust earthquake considering p, sv, and sh amplification transfer functions. *Bulletin of the Seismological Society of America*, 108(5), 2333–2346. https://doi.org/10.1785/0120170342.

Steidl, J., Tumarkin, A., & Archuleta, R. (1996). What is a reference site? *Bulletin of the Seismological Society of America*, 86(6): 1733-1748.

Wang, N., Takedatsu, T., Olsen, K., & Day, S. (2019). Broadband ground-motion simulation with interfrequency correlations. *Bulletin of the Seismological Society of America*, 109(6), 2437–2446. https://doi.org/10.1785/0120190136.